optica

Highly efficient scalable monolithic semiconductor terahertz pulse source

J. A. Fülöp,[1,2,3,*] Gy. Polónyi,[1,2] B. Monoszlai,[2,3] G. Andriukaitis,[4] T. Balciunas,[4] A. Pugzlys,[4,5] G. Arthur,[6] A. Baltuska,[4,5] and J. Hebling[1,2]

[1]MTA-PTE High-Field Terahertz Research Group, Pécs, Hungary
[2]Institute of Physics & Szentágothai Research Centre, University of Pécs, Pécs, Hungary
[3]ELI-ALPS, ELI-Hu Nkft., Szeged, Hungary
[4]Photonics Institute, Vienna University of Technology, Vienna, Austria
[5]Center for Physical Sciences & Technology, Vilnius, Lithuania
[6]Scitech Precision Ltd., Oxford, UK
*Corresponding author: fulop@fizika.ttk.pte.hu

Received 16 June 2016; revised 11 August 2016; accepted 17 August 2016 (Doc. ID 267263); published 21 September 2016

Intense pulses at low terahertz (THz) frequencies of 0.1–2 THz are an enabling tool for constructing compact particle accelerators and for strong-field control of matter. Optical rectification in lithium niobate provided sub-mJ THz pulse energies, but it is challenging to increase it further. Semiconductor sources suffered from low efficiency. Here, a semiconductor (ZnTe) THz source is demonstrated, collinearly pumped at an infrared wavelength beyond the three-photon absorption edge and utilizing a contact grating for tilting the pump-pulse front. Suppression of free-carrier absorption at THz frequencies in this way resulted in 0.3% THz generation efficiency, two orders of magnitude higher than reported previously from ZnTe. Scaling the THz energy to the mJ level is possible simply by increasing the pumped area. This unique THz source with excellent focusability, pumped by novel, efficient infrared sources, opens up new perspectives for THz high-field applications. © 2016 Optical Society of America

OCIS codes: (190.4360) Nonlinear optics, devices; (190.5970) Semiconductor nonlinear optics including MQW; (230.1950) Diffraction gratings; (300.6495) Spectroscopy, terahertz.

http://dx.doi.org/10.1364/OPTICA.3.001075

Terahertz (THz) pulses with high energy and field strength are enabling novel applications [1–4], including resonant control over ionic motion, bound and free electrons, as well as nonresonant and strong-field interactions [3]. Intense THz pulses hold promise for the development of a new generation of compact particle and x-ray sources [1,2]. Laser- and THz-driven particle accelerators with unprecedented flexibility can be important for free-electron lasers [2,5] and materials science and could revolutionize medical therapy with x-ray, electron, or proton beams [1,2].

Single-cycle or nearly single-cycle THz pulses with high energy can be generated by optical rectification of femtosecond laser pulses. The highest so far THz pulse energy reported from such a source, utilizing the novel organic nonlinear material DSTMS, was 0.9 mJ [6]. The spectrum obtained from organic materials is typically centered in the 2 to 10 THz range, well suited for nonlinear spectroscopic studies. THz sources with lower frequencies are optimally fitted to the requirements of particle acceleration [1,2,7]. The frequency range below 2 THz can be better accessed with another nonlinear material, lithium niobate, utilizing pump pulses with a tilted intensity front for non-collinear phase matching [8]. THz pulses with more than 0.4 mJ energy were generated with 0.77% efficiency using this technique [7]. However, increasing the THz energy further turned out to be very challenging because of the large pulse-front tilt angle (63°) and the associated large angular dispersion of the pump [9,10]. The effect of a strong THz field on the pump pulse, owing to their nonlinear interaction, leads to additional difficulties involving the reduction of the THz generation efficiency [11] and the distortion of the THz beam [12].

Semiconductor nonlinear materials have been extensively used to access the low-frequency part of the THz spectrum. The most popular material is ZnTe, where collinear phase matching is possible at the commonly used 0.8 μm pump wavelength of Ti:sapphire lasers. The highest THz pulse energy demonstrated so far from a semiconductor source was 1.5 μJ [13], where the efficiency was 3×10^{-5}. The reason for the low efficiency is the two-photon absorption (2PA) of the pump, which leads to the generation of free carriers and an increased absorption of THz radiation. Consequently, the useful pump intensity and the THz generation efficiency are limited [14]. The potential of long-wavelength pumping of semiconductors for high-energy THz pulse generation has been recognized only recently [9,15], though without demonstrating the scaling of THz energy beyond state of the art [13].

Here, a highly efficient, monolithic, and alignment-free semiconductor THz source is demonstrated. The source is pumped at an infrared wavelength beyond the three-photon absorption (3PA) edge. Such long-wavelength pumping enables

the suppression of 2PA and 3PA, together with the associated free-carrier absorption of THz radiation. The important consequence is that a higher pump intensity can be used and a higher THz generation efficiency can be achieved. At infrared wavelengths, semiconductors typically require tilting the pump-pulse front for phase matching [9,14,15]. It is shown here that a highly efficient semiconductor THz source can be constructed by using a contact grating (CG) for tilting the pump-pulse front [16–18]. This allows one to eliminate the distortions caused by imaging optics in conventional pulse-front tilting setups [9]. The small tilt angle, typically in the range of 20° to 30°, makes semiconductor materials ideally suited for the realization of a CG THz source.

The principle of operation of the semiconductor CG source is illustrated in Fig. 1(a). A grating structure, responsible for tilting the pump-pulse front, is formed on the entrance surface of the nonlinear material. In the setup shown here, the pump beam is perpendicularly incident on the CG and two symmetrically propagating diffraction orders $m = \pm 1$ are created [17,19]. The generated THz beam propagates collinearly with the incident pump beam and leaves the crystal through the back surface.

ZnTe was chosen as the nonlinear material because of its relatively large nonlinear coefficient ($d_{\text{eff}} = 68.5$ pm/V [20,21]), but the technique can easily be adopted to other semiconductors. The pump wavelength was 1.7 μm, which is above the 3PA edge of ZnTe. The pump pulse-front tilt angle was set by the grating period of 1275 nm to $\gamma \approx 28°$ for phase matching at 1 THz. The pump and THz polarization and propagation directions, as well as the orientations of the 2 mm-thick ZnTe substrate and the grating lines are shown in Fig. 1(b). The manufactured grating profile [see Figs. 1(c) and 1(d)] was closely fitted to the binary design profile, optimized for the highest diffraction efficiency [19]. For 50% filling factor, 400 nm profile depth, and TE polarization, about a 78% diffraction efficiency was predicted in total for the two orders $m = \pm 1$.

The CG with an area of 10 mm × 10 mm [Fig. 1(e)] was fabricated at Scitech Precision Ltd. using a combination of electron beam (e-beam) microlithography and dry (plasma) etching. Initially, the polished ZnTe substrate was coated with an etch-resistant metallic film, followed by a layer of e-beam resist. The resist was patterned by e-beam lithography. The pattern was transferred into the metal layer and subsequently into ZnTe in two different dry-etching steps. Finally, the residual metal was stripped, and the substrate cleaned and inspected before use. We note that bubbles in the substrate uncovered as pits in the surface resulted in the disruption of the resist film and caused defects of the grating profile (seen as light lines, parallel to the invisible grating lines, in Fig. 1(e); see also Supplement 1: Characterization of the contact-grating THz source). Such defects were affecting about 20% of the total grating area. A final grating in ZnTe at the correct dimensions could be created by taking into account the individual offsets and biases of the lithography and pattern transfer processes, and a careful optimization of the e-beam exposure was necessary during test runs. Nearly perpendicular wall angles could be achieved [Fig. 1(d)], which was important for a high diffraction efficiency.

The THz energy was measured by a calibrated pyroelectric detector (Gentec QS9-THZ-BL). A Teflon plate blocked the infrared pump and transmitted only the THz radiation to the detector. The voltage signal of the detector was fed to a storage oscilloscope, and the THz energy W_{THz} was calculated from the voltage modulation V_{m} of the recorded trace according to $W_{\text{THz}} = CV_{\text{m}}\tau/S$, where the sensitivity $S = 1.2$ kV/W was obtained from factory calibration, while the correction factor $C \approx 1$ and the time constant $\tau = 5.1$ ms were determined from the fitting of the recorded trace [7].

Up to 3.9 μJ THz pulse energy was observed from the CG source (Fig. 2, black circles), generated with 0.17% efficiency (Fig. 2, red squares) by using pump pulses of 144 fs duration, which were delivered by an optical parametric amplifier (OPA, see Supplement 1: Pump source). For comparison, the previously reported highest THz pulse energy from a semiconductor source was 1.5 μJ [13]. As high as 0.3% maximum conversion efficiency was achieved [Fig. 2(b)], corresponding to 2.3 μJ THz energy.

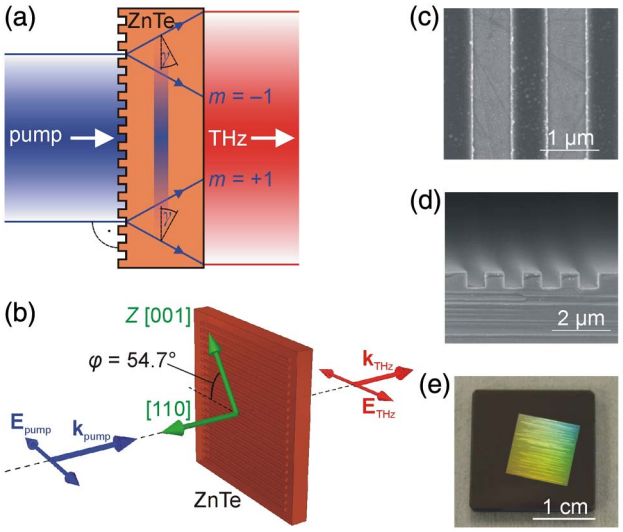

Fig. 1. (a) Scheme of the CG THz source with collinear geometry, utilizing the two diffraction orders $m = \pm 1$. The pulse-front tilt angle is γ. (b) Geometry of the CG THz source. $\mathbf{E}_{\text{pump}}$ and $\mathbf{E}_{\text{THz}}$: pump and THz polarization directions, $\mathbf{k}_{\text{pump}}$ and $\mathbf{k}_{\text{THz}}$: pump and THz propagation directions. Crystallographic directions are given in rectangular brackets. φ: angle between grating lines and the crystallographic Z-axis. (c) Top-down scanning electron microscope (SEM) image of the grating surface. (d) SEM micrograph of a cleaved test sample showing the grating profile. (e) Photograph of the CG THz source.

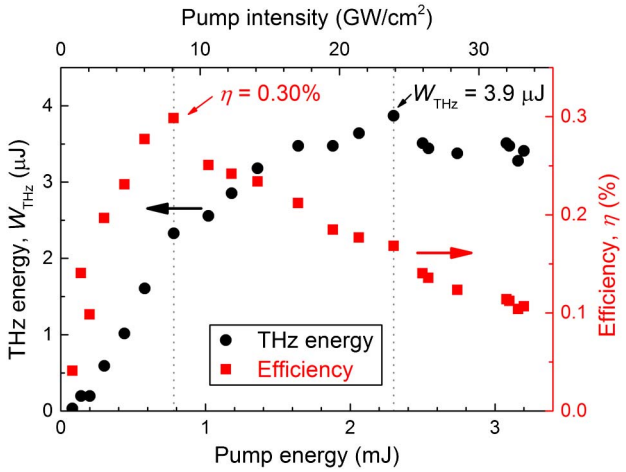

Fig. 2. Measured THz energy (black circles) and THz generation efficiency (red squares) versus pump energy and intensity.

This efficiency is 6 times higher than the highest value reported previously from any semiconductor source [15] and 97 times higher than the highest previously reported value for a ZnTe source [13]. The former was achieved with GaAs, pumped above the 2PA, but below the 3PA edge [15], and the latter was achieved with ZnTe pumped collinearly at 0.8 μm, suffering from strong 2PA. We note that in a lithium niobate CG source, partly because of technical reasons, only a very small THz generation efficiency (1.5×10^{-4}) was demonstrated so far [18]. The potential of the semiconductor CG THz source is clearly demonstrated here by the significant increase both in energy and efficiency.

One important consequence of the collinear setup geometry is the very good focusability of the THz beam. This is illustrated by the pyroelectric camera (Ophir Spiricon, Pyrocam III) image of the THz focal spot (Fig. 3), where the relative deviation of the spot size from the estimated diffraction limit was only about 15%. For estimating the diffraction limit, Gaussian beam propagation was assumed with an initial THz spot size at the CG equal to that of the pump. The estimation of the initial THz spot size corresponds to a linear, rather than a quadratic, dependence of the THz energy on pump energy, justified by the observed saturation of the THz generation (Fig. 2).

Electro-optic sampling (EOS) using a (110)-cut ZnTe crystal of 0.1 mm thickness, placed in contact with a 2 mm thick inactive substrate, revealed a nearly single-cycle THz waveform [Fig. 4(a)]. A small fraction of the 200-fs pulses driving the OPA at 1.03 μm wavelength were used as the sampling pulses. The peak electric field was about 0.57 MV/cm, as estimated from the measured 3.9 μJ pulse energy, 2.1 mm^2 focal spot size, and the waveform in Fig. 4(a). Fourier transform spectroscopy was used to measure the THz spectrum in order to avoid distortions due to the relatively long sampling pulses. For this purpose, the field autocorrelation [AC, Fig. 4(b)] was recorded with a Michelson interferometer containing a silicon beam splitter and the pyroelectric

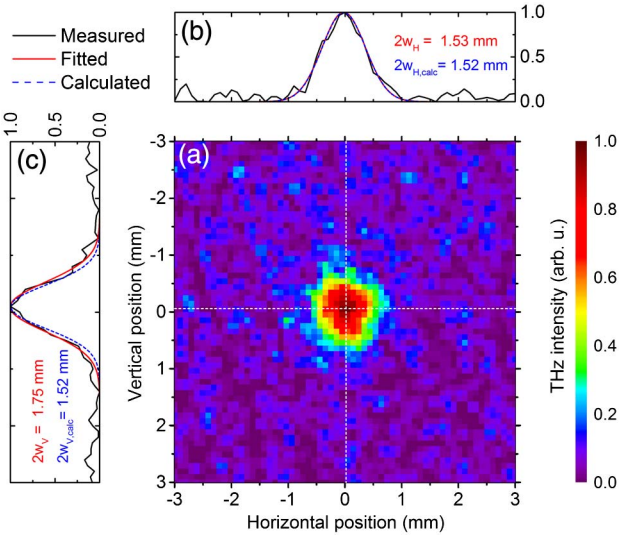

Fig. 3. (a) Pyroelectric camera image of the THz beam in the focus of a 10 cm focal length Teflon lens placed at a 50 cm distance behind the CG source. The pump energy was 1.2 mJ. Black solid lines in (b) and (c) show the horizontal and vertical cross sections of the THz beam profile along the white dashed lines in (a), respectively. Red solid lines: Gaussian fit. Blue dashed lines: estimated diffraction-limited profiles. w_H, w_V, $w_{H,\mathrm{calc}}$, $w_{V,\mathrm{calc}}$: horizontal and vertical fitted and calculated beam radii at $1/e^2$ of the peak intensity.

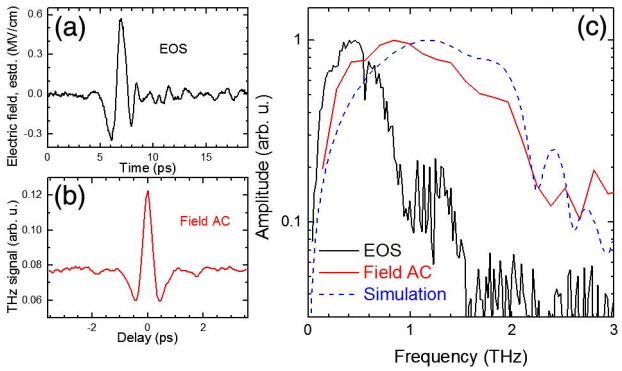

Fig. 4. (a) Temporal waveform of the THz pulses measured by EOS at 2.4 mJ pump energy. (b) Field AC of the THz pulses measured by a Michelson interferometer at a 1.8 mJ pump energy. (c) Spectral amplitude of the THz pulses obtained by Fourier transformation from EOS (black solid line) and field AC (red solid line) and from the simulation (blue dashed line).

energy meter as the detector. The THz spectrum was obtained by Fourier transformation of the interferogram. The maximum of the spectral intensity was at 0.9 THz, and the spectrum extended up to about 2.3 THz [Fig. 4(c)].

The scalability of the CG THz source to higher energies and field strengths is important for applications. In this experiment, about 20% of the grating surface was ineffective due to defects in the substrate [seen as light lines in Fig. 1(e)]. A better substrate quality can eliminate such efficiency-reducing defects. Most importantly, scaling to higher energies is possible simply by increasing the pumped area and the pump energy. A segmented source, similar to organic crystals [22], could be used to circumvent possible limitations of the substrate size and grating manufacturing technology. Another possibility is to increase the efficiency by increasing the material thickness. Calculations predict 2.3 × (3.7 ×) higher efficiency by doubling (tripling) the substrate length [Fig. 5(a), see also Supplement 1: Simulation of THz generation]. The expectation of an increased efficiency is supported by our measurements using a conventional (external) pulse-front tilting setup to pump a prism-shaped ZnTe crystal of 1.5 × larger average (center) thickness than that of the CG. As high as 0.7% maximum conversion efficiency and 6.6 μJ THz energy were measured at a 15 GW/cm^2 pump intensity. Furthermore, cooling the crystal reduces the THz absorption and can enhance the spectral amplitude especially above 1 THz, where ZnTe absorbs stronger [Fig. 5(b) and Supplement 1, Fig. S4]. Crystals with smaller absorption and dispersion, such as GaP, can be more advantageous for generating high field strengths (Fig. 5 and Supplement 1, Figs. S4 and S5). A more detailed discussion of the simulation results, including those in Fig. 5, can be found in Section 3 of Supplement 1.

In summary, a compact, monolithic, and alignment-free THz source was demonstrated. It utilizes a semiconductor nonlinear material pumped beyond the three-photon absorption edge and a contact grating for tilting the pump-pulse front. The collinear setup geometry is of great advantage for user experiments and ensures an excellent focusability of the THz beam. The efficiency demonstrated with the ZnTe CG source was as much as 6 times higher than the highest previously reported value from any semiconductor THz source and the enormous two orders of magnitude higher than previously reported from a ZnTe source.

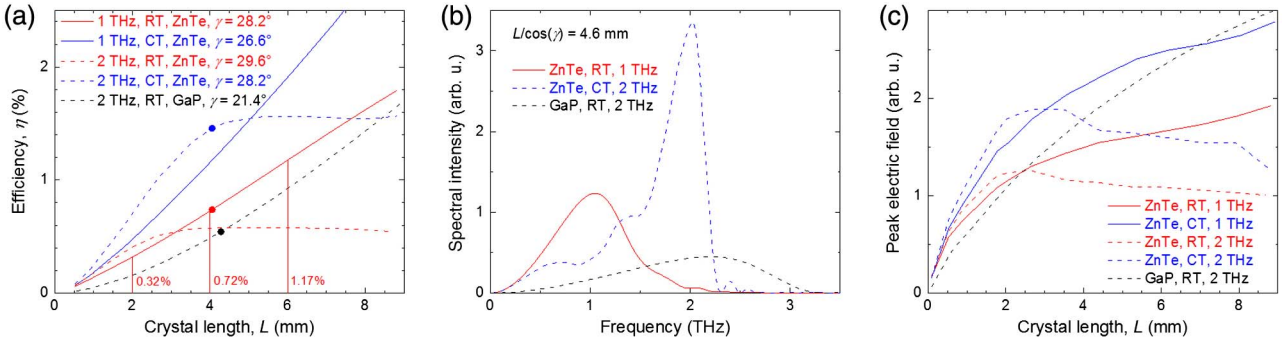

Fig. 5. Simulation of THz generation. (a) Scaling of THz generation efficiency with the crystal length in ZnTe for 1 THz (solid lines) and 2 THz (dashed lines) phase-matching frequencies at room temperature (RT, red lines) and the cryogenic temperature of 80 K (CT, blue lines). In the calculation, a 1.7 μm pump wavelength, 144 fs pulse duration, and 8.1 GW/cm^2 pump intensity were assumed, the latter corresponding to the maximum of the measured efficiency (Fig. 2). Vertical lines correspond to the crystal length of 2 mm used in the experiment and its multiples (2 ×, 3 ×). The black dashed line shows the result of a similar calculation for GaP at RT with 2 THz phase-matching frequency. The respective pulse-front tilt angles are given in the plot legend. (b) Examples of calculated THz spectra, corresponding to parameters indicated by symbols in (a). (c) Calculated scaling of the peak electric field with the crystal length.

The observed high efficiencies, similar to values reported for lithium niobate at high pulse energies [7], clearly demonstrate the potential of semiconductors as future high-energy THz pulse sources and support the expectation that THz pulses with 1 mJ energy can be generated with less than 200 mJ pump energy from a (possibly segmented) CG source of about a 5 cm diameter. This new type of THz source, in combination with novel, efficient, infrared pump sources in the 1.7 to 2.5 μm wavelength range based, for example, on Holmium laser technology [23], opens up new perspectives for THz high-field applications. These range from strong-field control of matter to compact sources of particle and x-ray beams and key technologies for medicine and materials science.

Funding. Hungarian Scientific Research Fund (OTKA) (113083); Hungarian Academy of Sciences (MTA) (János Bolyai Research Scholarship to J. A. Fülöp); Austrian Science Fund (FWF) (SFB NextLite F4903-N23, P 26658).

Acknowledgment. The help of G. Almási, Z. Ollmann, Cs. Lombosi, and T. Kanai is acknowledged. The present scientific contribution is dedicated to the 650th anniversary of the foundation of the University of Pécs, Hungary.

See Supplement 1 for supporting content.

REFERENCES

1. L. Pálfalvi, J. A. Fülöp, Gy. Tóth, and J. Hebling, Phys. Rev. ST Accel. Beams **17**, 031301 (2014).
2. E. A. Nanni, W. R. Huang, K.-H. Hong, K. Ravi, A. Fallahi, G. Moriena, R. J. D. Miller, and F. X. Kärtner, Nat. Commun. **6**, 8486 (2015).
3. T. Kampfrath, K. Tanaka, and K. A. Nelson, Nat. Photonics **7**, 680 (2013).
4. L. V. Titova, A. K. Ayesheshim, A. Golubov, R. Rodriguez-Juarez, R. Woycicki, F. A. Hegmann, and O. Kovalchuk, Sci. Rep. **3**, 2363 (2013).
5. J. Hebling, J. A. Fülöp, M. I. Mechler, L. Pálfalvi, C. Tőke, and G. Almási, "Optical manipulation of relativistic electron beams using THz pulses," arXiv:1109.6852 (2011).
6. C. Vicario, A. V. Ovchinnikov, S. I. Ashitkov, M. B. Agranat, V. E. Fortov, and C. P. Hauri, Opt. Lett. **39**, 6632 (2014).
7. J. A. Fülöp, Z. Ollmann, Cs. Lombosi, C. Skrobol, S. Klingebiel, L. Pálfalvi, F. Krausz, S. Karsch, and J. Hebling, Opt. Express **22**, 20155 (2014).
8. J. Hebling, G. Almási, I. Z. Kozma, and J. Kuhl, Opt. Express **10**, 1161 (2002).
9. J. A. Fülöp, L. Pálfalvi, G. Almási, and J. Hebling, Opt. Express **18**, 12311 (2010).
10. J. A. Fülöp, L. Pálfalvi, M. C. Hoffmann, and J. Hebling, Opt. Express **19**, 15090 (2011).
11. K. Ravi, W. R. Huang, S. Carbajo, X. Wu, and F. Kärtner, Opt. Express **22**, 20239 (2014).
12. Cs. Lombosi, Gy. Polónyi, M. Mechler, Z. Ollmann, J. Hebling, and J. A. Fülöp, New J. Phys. **17**, 083041 (2015).
13. F. Blanchard, L. Razzari, H.-C. Bandulet, G. Sharma, R. Morandotti, J.-C. Kieffer, T. Ozaki, M. Reid, H. F. Tiedje, H. K. Haugen, and F. A. Hegmann, Opt. Express **15**, 13212 (2007).
14. M. Hoffmann, K.-L. Yeh, J. Hebling, and K. A. Nelson, Opt. Express **15**, 11706 (2007).
15. F. Blanchard, B. E. Schmidt, X. Ropagnol, N. Thiré, T. Ozaki, R. Morandotti, D. G. Cooke, and F. Légaré, Appl. Phys. Lett. **105**, 241106 (2014).
16. L. Pálfalvi, J. A. Fülöp, G. Almási, and J. Hebling, Appl. Phys. Lett. **92**, 171107 (2008).
17. M. I. Bakunov and S. B. Bodrov, J. Opt. Soc. Am. B **31**, 2549 (2014).
18. M. Tsubouchi, K. Nagashima, F. Yoshida, Y. Ochi, and M. Maruyama, Opt. Lett. **39**, 5439 (2014).
19. Z. Ollmann, J. A. Fülöp, J. Hebling, and G. Almási, Opt. Commun. **315**, 159 (2014).
20. J. Hebling, K.-L. Yeh, M. C. Hoffmann, B. Bartal, and K. A. Nelson, J. Opt. Soc. Am. B **25**, B6 (2008).
21. Q. Wu and X.-C. Zhang, Appl. Phys. Lett. **68**, 1604 (1996).
22. C. Vicario, B. Monoszlai, and C. P. Hauri, Phys. Rev. Lett. **112**, 213901 (2014).
23. P. Malevich, G. Andriukaitis, T. Flöry, A. J. Verhoef, A. Fernández, S. Alisauskas, A. Pugzlys, A. Baltuska, L. H. Tan, C. F. Chua, and P. B. Phua, Opt. Lett. **38**, 2746 (2013).

160.114.157.148 {ts '2023-05-15 09:27:17'}